

CHAPTER 4: THE BINDING OF $\text{Ru}(\text{BPY})_2(\text{EILATIN})^{2+}$ TO MATCHED AND MISMATCHED DNA^Ψ

4.1: INTRODUCTION

The success and potential of the first generations of metalloinsertors have spurred considerable efforts to expand the family of compounds.^{1,2} To this end, over the past ten years, our laboratory has developed mismatch-specific complexes featuring different metal centers³, inserting ligands⁴, and ancillary ligands.⁵⁻⁹ Importantly, this variation provides an opportunity to exploit both the structure and reactivity of new molecular components. Further, the inherent modularity of metal complexes has made many of these alterations, especially those involving ancillary ligands, relatively facile.

The recent revelation of the detailed structure of metalloinsertion at a single base mismatch has further informed the drive for innovation.^{10,11} Traditional metallointercalators such as $\text{Rh}(\text{bpy})_2(\text{phi})^{3+}$ bind DNA from the major groove, stacking a planar, aromatic ligand between adjacent base pairs and thus doubling the helical rise.¹²⁻¹⁷ In contrast, $\text{Rh}(\text{bpy})_2(\text{chrysi})^{3+}$ and other metalloinsertors bind their target sites from the minor groove by extruding the mismatched bases into the major groove and replacing the displaced bases in the helical π -stack with their sterically expansive ligand (**Figure 4.1**). This binding is accommodated by a slight widening of the phosphate backbone at the mismatched site.

Prior to elucidating this structure, we had reported a direct correlation between the specific binding affinity of a metalloinsertor and the thermodynamic destabilization of its

^Ψ Adapted from Zeglis, B. M.; Barton, J. K. Binding of $\text{Ru}(\text{bpy})_2(\text{eilatin})^{2+}$ to matched and mismatched DNA. *Inorg. Chem.* **2008**, *47*, 6452–5457.

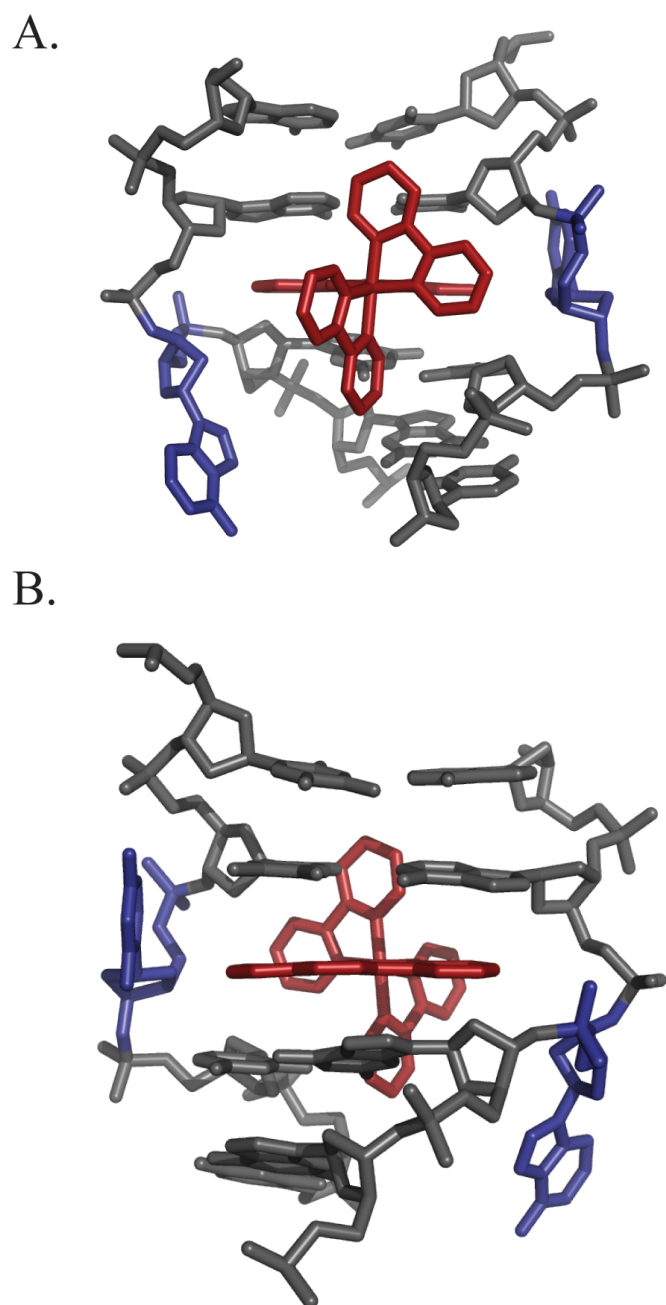


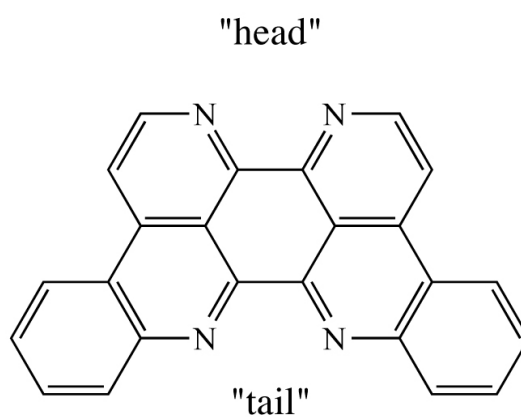
Figure 4.1: Structure of metalloinsertion at a C•A mismatch.¹¹ Views of metalloinsertion from the minor (A) and major (B) groove sides of the target site.

target site (see Chapter 1).¹⁸⁻²¹ More destabilized mismatches are bound more tightly than less destabilized sites, with highly stable, G-containing sites escaping recognition altogether. The extrusion of the mispaired bases by a metalloinsertor provides a clear explanation for this behavior: the less stable the mismatch, the more easily it is extruded from the helix by a metalloinsertor.

One of the primary objectives in the synthesis and study of novel metalloinsertors is the development of mismatch-specific complexes that target the elusive, more stable mismatches. In pursuit of this goal, we considered that augmenting the size of the bulky aromatic ligand might provide this increase in the range of mismatches targeted, an idea predicated on the notion that greater surface area for π -stacking might yield the boost in binding affinity needed for the recognition of more thermodynamically stable mismatched sites. Herein, we report investigations into the DNA-binding properties of $\text{Ru}(\text{bpy})_2(\text{eilatin})^{2+}$, a complex bearing an exceptionally expansive ligand (**Figure 4.2**).²²

Eilatin is a highly symmetric, heptacyclic natural product from the pyrido[2,3,4-*kl*]acridine family of marine alkaloids. It was first isolated in 1988 from the tunicate *Eudistoma sp.* in the Gulf of Eilat in the Red Sea.²³ While the molecule itself has proven of significant interest both to synthetic^{24, 25} and biological²⁶⁻³⁰ chemists, it is, however, eilatin as a ligand in an octahedral metal complex that offers the possibility of high-affinity metalloinsertion.^{22, 31} Indeed, the maximum width of the coordinated eilatin ligand is 13.3 Å, compared to 11.8 Å for the mismatch-specific chrysene-5,6-quinone diimine (chrysi) ligand and 9.2 Å for the non-specific 9,10-phenanthrenequinone diimine (ϕ) ligand (**Figure 4.3**).³² Moreover, the eilatin ligand contains seven aromatic rings

A.



B.

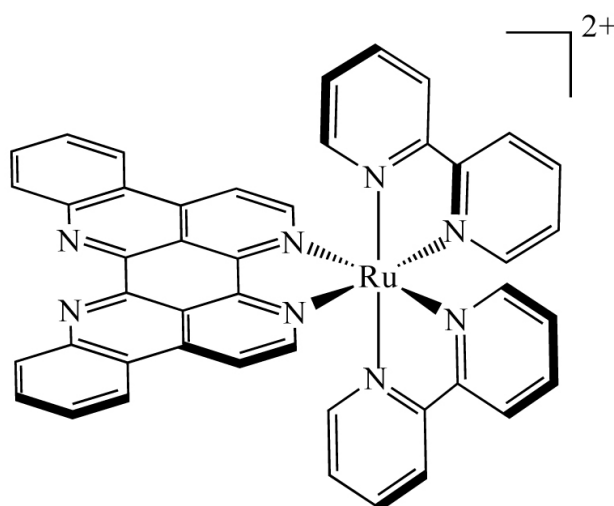


Figure 4.2: Eilatin and $\text{Ru}(\text{bpy})_2(\text{eilatin})^{2+}$. The structures of (A) eilatin and (B) $\text{Ru}(\text{bpy})_2(\text{eilatin})^{2+}$

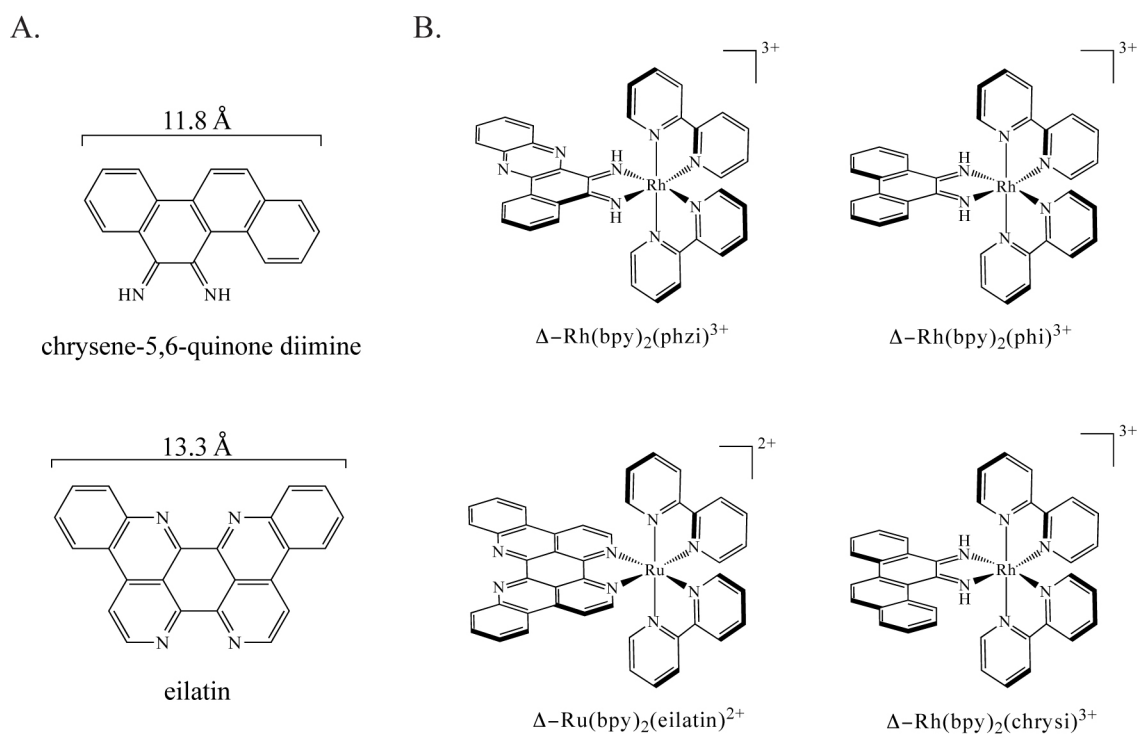


Figure 4.3: Comparison of eilatin to other DNA-binding ligands. (A) The widths of chrysene-5,6-quinone diimine and eilatin, as approximated using ChemDraw3D with energy-minimized structures. (B) The structures of four DNA-binding metal complexes: a metallointercalator, Rh(bpy)₂(phi)³⁺; two metalloinsertors, Rh(bpy)₂(chrysi)³⁺ and Rh(bpy)₂(phzi)³⁺; and the complex under investigation, Ru(bpy)₂(eilatin)²⁺.

available for π -stacking upon insertion into the DNA helix; the chrysi ligand, for comparison, has only four. It is our hypothesis that the singular expanse of the eilatin ligand makes $\text{Ru}(\text{bpy})_2(\text{eilatin})^{2+}$ a tremendously attractive candidate for a high affinity, mismatch-specific metalloinsertor.

$\text{Ru}(\text{bpy})_2(\text{eilatin})^{2+}$ has been previously prepared and characterized spectroscopically by Kol and coworkers.^{22, 31, 33-35} Moreover, studies with nucleic acids by Tor and coworkers have revealed binding to folded RNAs and non-specific association with calf thymus DNA.³⁶⁻³⁸ It is of note here that in investigating the DNA-binding properties of $\text{Ru}(\text{bpy})_2(\text{eilatin})^{2+}$, we are departing from the well-studied $\text{Rh}(\text{bpy})_2(\text{chrysi})^{3+}$ system on two fronts, both the metal and the inserting ligand. Our laboratory has previously examined the binding of luminescent ruthenium complexes to DNA and RNA, most notably the light-switch compound $\text{Ru}(\text{phen})_2(\text{dppz})^{2+}$.^{39, 40} Yet here, our interest is primarily derived from the shape characteristics of the ligand and its potential applications as a specific probe for mismatched DNA. Our studies show, however, that steric bulk alone is insufficient to achieve site-specificity.

4.2: RESULTS AND DISCUSSION

4.2.1: SYNTHESIS AND CHARACTERIZATION

Eilatin was synthesized according to the biomimetic route published by Gellerman and coworkers (**Figure 4.4a**).⁴¹⁻⁴³ Kynuramine, a natural product in its own right, was first protected via trifluoroacetylation using ethyl trifluoroacetate in methanol. The protected product was then reacted with catechol under oxidative conditions (EtOH, NaIO_3) to form a 1,2-acridinedione derivative intermediate. This intermediate was

purified via column chromatography (9:1 CHCl₃:MeOH, SiO₂) and then treated with base to catalyze the cyclization reaction that yields a yellow fluorescent product: eilatin. While the synthetic transformations may seem somewhat convoluted, an alignment of the precursors makes quite clear the origins of the molecule's carbon and nitrogen skeleton (**Figure 4.4b**).

The metallation of the eilatin ligand onto ruthenium was also performed according to published procedures. A solution of Ru(bpy)₂(Cl)₂ and eilatin in 1:1 MeOH:H₂O was refluxed for five hours to yield the desired product: Ru(bpy)₂(eilatin)²⁺.²² The complex was isolated from the reaction mixture via precipitation with NH₄PF₆, and the hexafluorophosphate anions were subsequently exchanged for chlorides via anion exchange chromatography. The final product was purified via reverse-phase HPLC using an HP1100 HPLC system, a Varian DynaMax C18 semipreparative column, and an elution gradient of 85:15 to 40:60 H₂O (0.1% TFA):MeCN (0.1% TFA) over 60 min. It is important to note that the metallation of eilatin is face-selective; only the sterically congested "head" of the ligand readily binds metals under most conditions. Far more forcing reactions are required to make 2:1 metal:eilatin complexes.³³

The spectroscopic properties of Ru(bpy)₂(eilatin)²⁺ are particularly interesting. Easily the most notable feature of the complex is its beautiful dark green color, a consequence of a broad ligand π-π* absorption band centered around 520 nm and an extremely low energy d_π(M)-π*(L) MLCT centered at 600 nm (**Figure 4.6**).

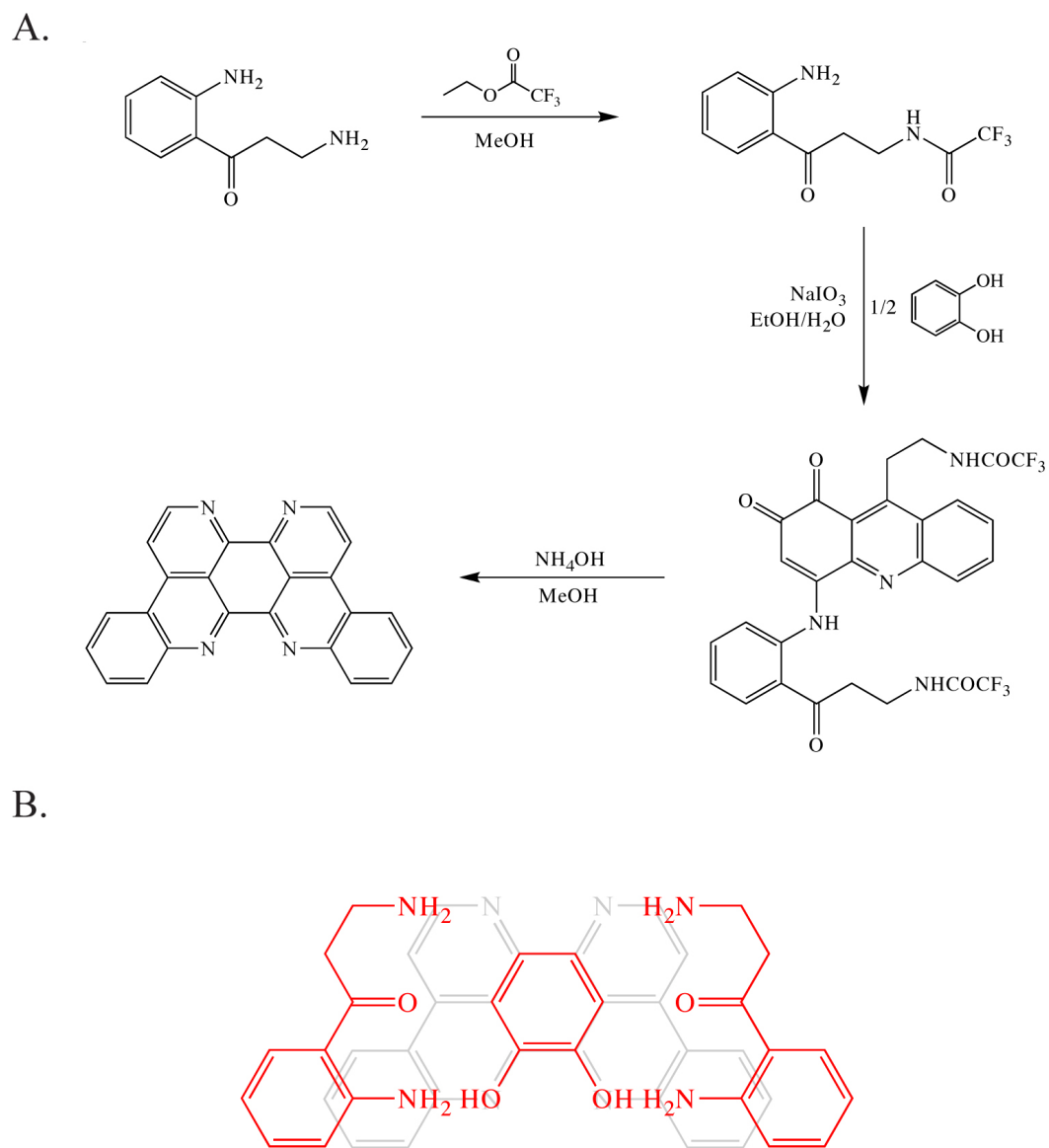


Figure 4.4: The synthesis of eilatin. (A) Eilatin can be synthesized via a biomimetic pathway in three steps from the natural product kynuramine. (B) An overlay of the starting materials and the product makes clear the origins of the carbon and nitrogen atoms in the molecule.

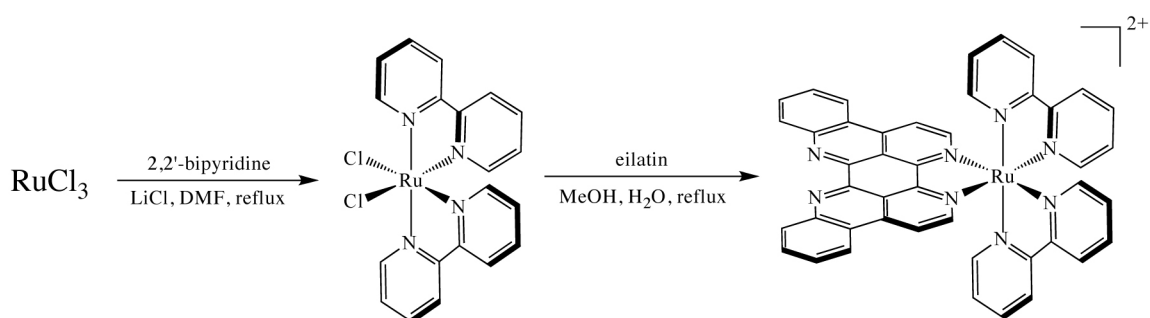


Figure 4.5: The synthesis of $\text{Ru}(\text{bpy})_2(\text{eilatin})^{2+}$. The metallation of the eilatin ligand is face-selective. Far harsher reaction conditions are required to prompt a metal to bind to the more sterically constrictive “tail” of the molecule.

Perhaps not surprisingly given the expense of the ligand, dimerization, in particular homochiral association, of $\text{Ru}(\text{bpy})_2(\text{eilatin})^{2+}$ has been observed by other groups.^{34, 35, 44, 45} As a consequence, UV-Vis spectroscopy was also used to probe this phenomenon in the concentration regimes relevant to the investigation. Fortunately, spectrophotometric titrations of the complex over the salient range of concentrations reveal no deviations from Beer's Law, indicating that dimer- and oligomerization are of little import in the study at hand.

4.2.2: INVESTIGATING THE SITE-SPECIFICITY OF $\text{Ru}(\text{BPY})_2(\text{EILATIN})^{2+}$

Owing to the short excited state lifetime of $\text{Ru}(\text{bpy})_2(\text{eilatin})^{2+}$, direct methods such as DNA photocleavage or singlet oxygen sensitization could not be used to characterize the sites targeted by the Ru complex within the DNA duplex.⁴⁶ Instead, competition experiments were employed. We first utilized $\text{Rh}(\text{bpy})_2(\text{phi})^{3+}$, which binds duplex DNA with little site-selectivity⁴⁷, in order to probe the binding sites of the Ru complex through competitive inhibition. A synthetic 33-mer oligonucleotide was synthesized with complements featuring a guanine (EL-M) or a cytosine (EL-MM) across from a central cytosine (bold) to form matched and mismatched strands: 5'-CGC TAC GTC TAT ATG CAT GAT CCT AAG TGA CAG TAC-3'. After synthesis and purification, the forward strand (shown) was radioactively labeled with ^{32}P at its 5'-terminus via standard protocols. Then, samples (1 μM) of radiolabeled EL-M and EL-MM DNA in buffer (50 mM NaCl, 10 mM NaPi, pH 7.1) were incubated with 8 μM

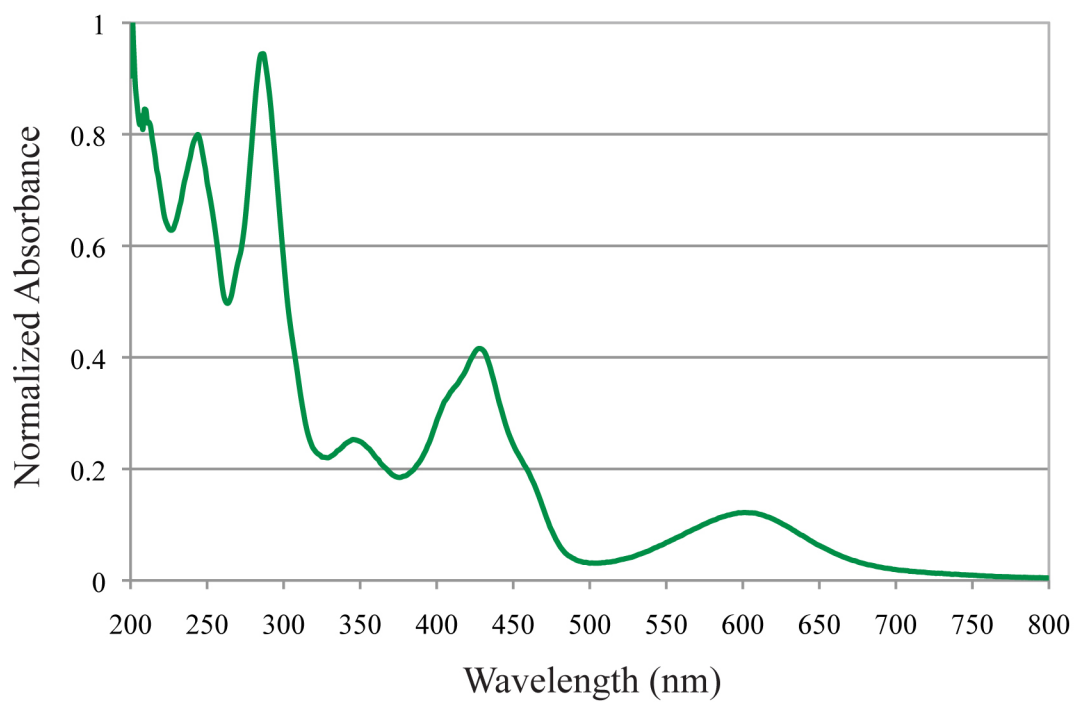


Figure 4.6: UV-Vis spectrum of Ru(bpy)₂(eilatin)²⁺. Extinction coefficients (H₂O, pH 7.0): λ_{\max} 244 nm ($\epsilon = 64,000$), 287 nm ($\epsilon = 68,000$), 426 nm ($\epsilon = 38,000$).

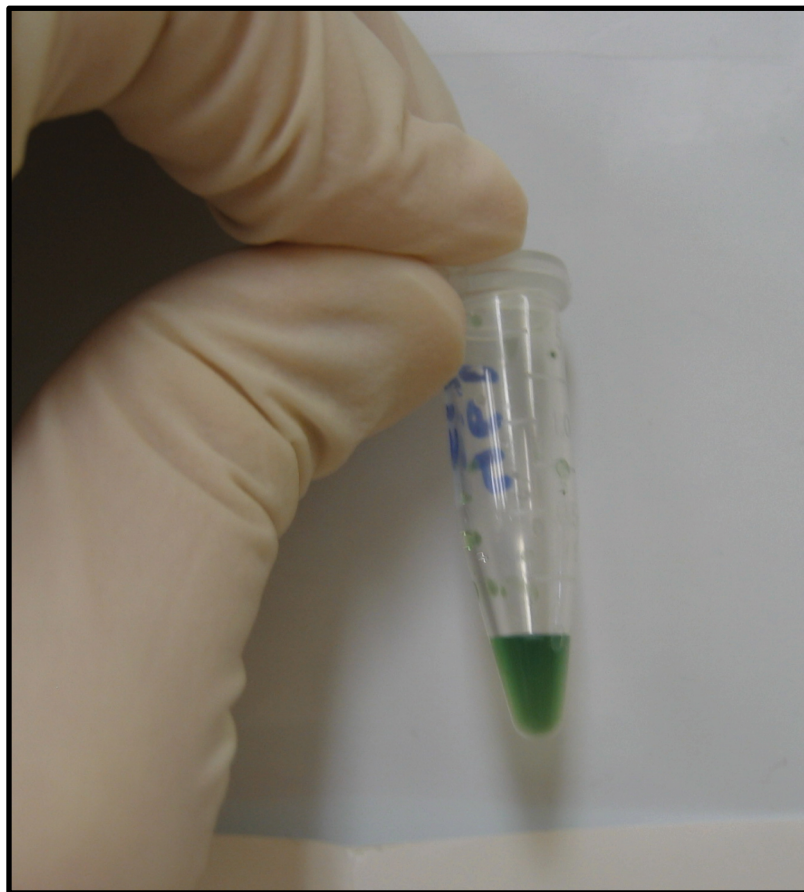


Figure 4.7: The distinctive green color of $\text{Ru}(\text{bpy})_2(\text{eilatin})^{2+}$. The solution shown is approximately 200 μM .

$\text{Rh}(\text{bpy})_2(\text{phi})^{3+}$ and irradiated for 20 minutes in the presence of variable amounts of $\text{Ru}(\text{bpy})_2(\text{eilatin})^{2+}$ using a solar simulator. A concentration of 8 μM $\text{Rh}(\text{bpy})_2(\text{phi})^{3+}$ provides 1 rhodium molecule per 4 base pairs, enough to saturate the entire oligonucleotide with rhodium complexes. Because previously published reports revealed few enantiomeric trends in the binding of $\text{Ru}(\text{bpy})_2(\text{eilatin})^{2+}$ to well-matched oligonucleotides, a racemic mixture of the Δ - and Λ -isomers was employed in all experiments. Moreover, while the dimerization of $\text{Ru}(\text{bpy})_2(\text{eilatin})^{2+}$ in solution has been observed, spectrophotometric titrations of the complex over the relevant range of concentrations reveal no deviations from Beer's Law, indicating that dimer- and oligomerization are of little import in the study at hand.

Autoradiography of the resultant gel reveals that $\text{Rh}(\text{bpy})_2(\text{phi})^{3+}$ promotes photocleavage on the EL-M DNA at six discrete sites (with base numbers from the 3'-end): C19, G22, C27, C29, T32, and C33 (**Figure 4.8**). Interestingly, EL-MM DNA is cleaved at the same locations by $\text{Rh}(\text{bpy})_2(\text{phi})^{3+}$ but also displays two more cleavage bands: T13 and C16. The C16 position is the mismatched site. The somewhat curious cleavage at T13 may result from local conformational changes created by the nearby mismatch in the EL-MM sequence, leading to hyper-reactivity.⁴⁸

The effect of increasing $\text{Ru}(\text{bpy})_2(\text{eilatin})^{2+}$ concentrations on $\text{Rh}(\text{bpy})_2(\text{phi})^{3+}$ photocleavage are also manifest in the gel (**Figures 4.8–4.10**). With increasing concentrations of $\text{Ru}(\text{bpy})_2(\text{eilatin})^{2+}$, all of the $\text{Rh}(\text{bpy})_2(\text{phi})^{3+}$ cleavage bands lessen in intensity on both the matched and mismatched duplexes, indicating that $\text{Ru}(\text{bpy})_2(\text{eilatin})^{2+}$ is competing with, and eventually inhibiting, rhodium binding at all sites.

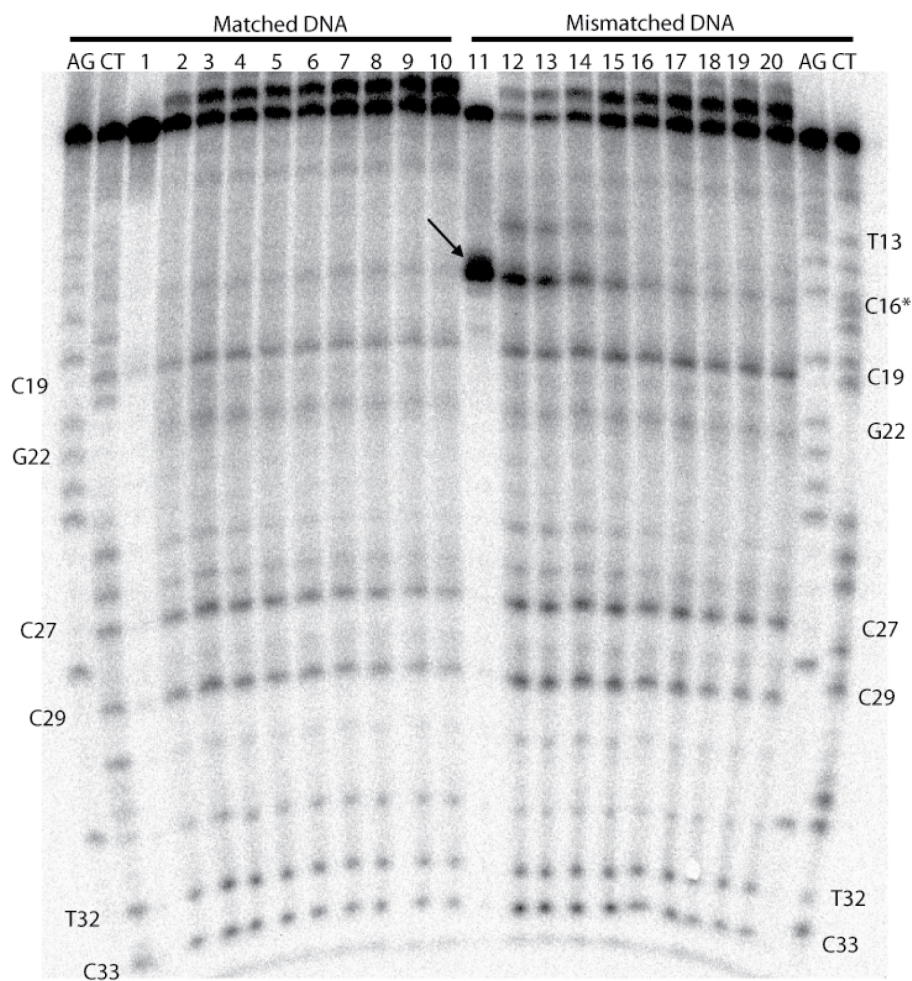


Figure 4.8: $\text{Rh}(\text{bpy})_2(\text{phi})^{3+}$ vs. $\text{Ru}(\text{bpy})_2(\text{eilatin})^{2+}$ competition gel. Denaturing polyacrylamide gel showing the competition of $\text{Rh}(\text{bpy})_2(\text{phi})^{3+}$ and $\text{Ru}(\text{bpy})_2(\text{eilatin})^{2+}$ for matched and mismatched DNA of the sequence 3'-GCGATGCAGATATACTACTAGGATTCAGTTCATG-³²P-5' (the italicized C is opposite a G in the matched duplex, in the mismatched sequence a C). All samples were prepared with 1 μM DNA, 50 mM NaCl, 10 mM NaPi, pH 7.1 and, unless otherwise stated, irradiated for 20 minutes on a solar simulator. Left and right AG and CT lanes are Maxam-Gilbert sequencing reactions for matched and mismatched DNA, respectively. Lanes 1–10 employ matched DNA, lanes 11–20 mismatched DNA. Sample conditions: lanes 1 and 11, 1 μM $\text{Rh}(\text{bpy})_2(\text{chrysi})$; lanes 2–10 and 12–20, 8 μM $\text{Rh}(\text{bpy})_2(\text{phi})^{3+}$. Lanes 3–10 and 13–20 also contain increasing amounts of $\text{Ru}(\text{bpy})_2(\text{eilatin})^{2+}$, beginning with 2.5 μM $\text{Ru}(\text{bpy})_2(\text{eilatin})^{2+}$ in lanes 3 and 13 and increasing in increments of 2.5 μM to 22.5 μM in lanes 10 and 20. The arrow marks the mismatched site.

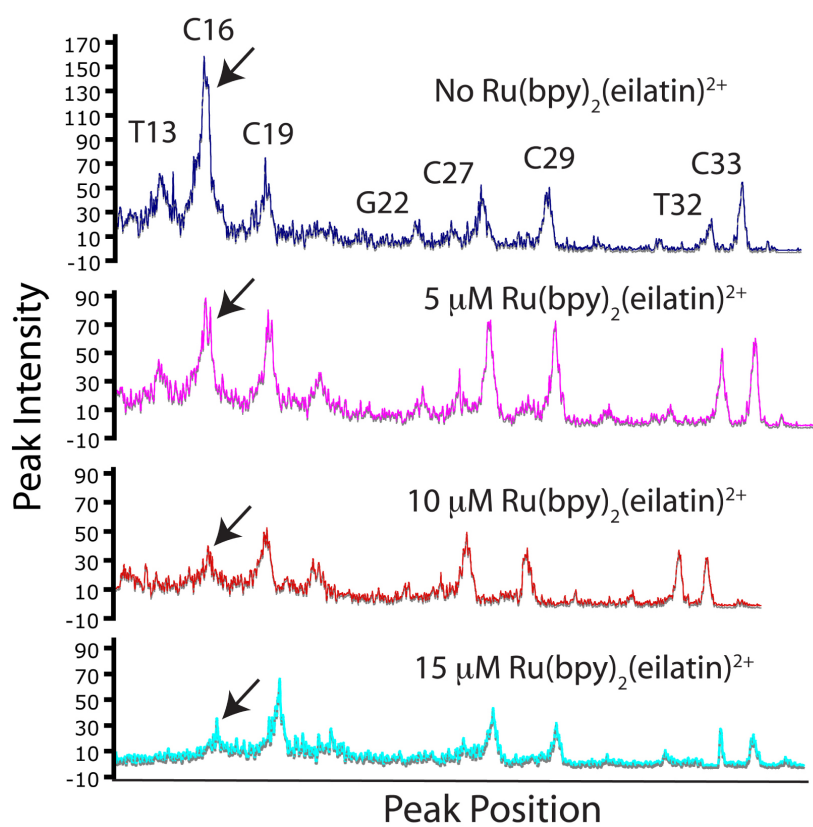


Figure 4.9: $\text{Rh}(\text{bpy})_2(\text{phi})^{3+}$ vs. $\text{Ru}(\text{bpy})_2(\text{eilatin})^{2+}$ competition experiment. Line plots of lanes 14, 16, 18, and 20 in the competition gel. The arrow marks the mismatched site.

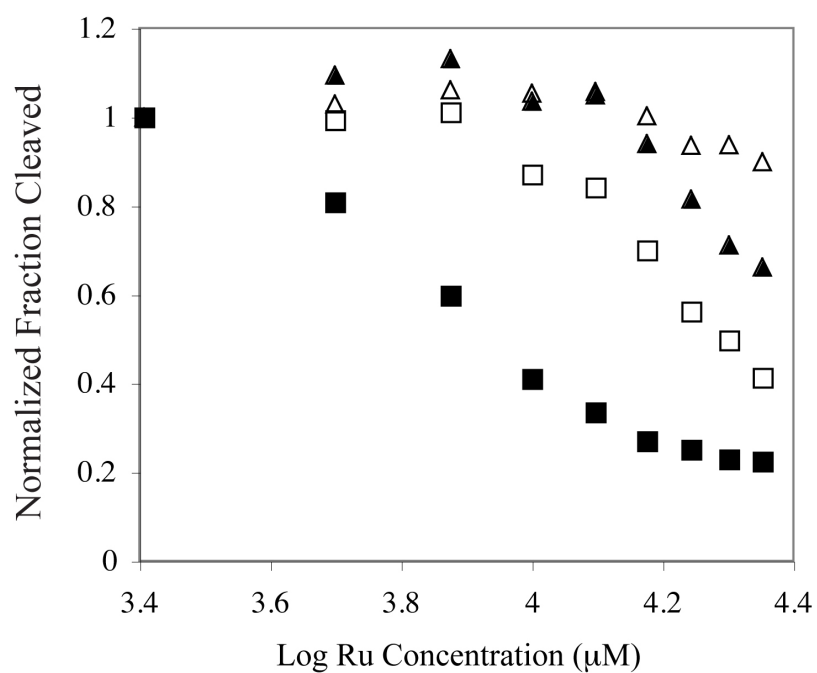


Figure 4.10: Rh(bpy)₂(phi)³⁺ vs. Ru(bpy)₂(eilatin)²⁺ competition experiment.

Quantitation of Rh(bpy)₂(phi)³⁺ cleavage band intensity is shown as a function of Ru(bpy)₂(eilatin)²⁺ concentration. Filled square represents C16; empty square, C29; filled triangle, C27; empty triangle, C19.

At these Ru concentrations, this non-specific inhibition of Rh photocleavage cannot be accounted for primarily through light absorption by the Ru complex but instead must reflect competitive binding of the Ru complex to well-matched DNA sites. Increasing concentrations of $\text{Ru}(\text{bpy})_3^{2+}$, a metal complex that binds DNA very weakly and has extinction coefficients similar to $\text{Ru}(\text{bpy})_2(\text{eilat})^{2+}$ over the spectral range of interest, have no effect on the photocleavage intensities of $\text{Rh}(\text{bpy})_2(\text{phi})^{3+}$ and $\text{Rh}(\text{bpy})_2(\text{chrysi})^{3+}$ in the salient concentration range (**Figure 4.11**). Importantly, this $\text{Ru}(\text{bpy})_3^{2+}$ control also helps to exclude the possibility that $\text{Ru}(\text{bpy})_2(\text{eilat})^{2+}$ reduces metallointercalator and metalloinsertor photocleavage via quenching of the rhodium excited state. For the well-matched duplex, photocleavage with 8 mM $\text{Rh}(\text{bpy})_2(\text{phi})^{3+}$ is fully inhibited at ~15 mM $\text{Ru}(\text{bpy})_2(\text{eilat})^{2+}$. Non-specific duplex binding occurring in the micromolar range is thus comparable for the two complexes.

Interestingly, however, site preferences for both $\text{Rh}(\text{bpy})_2(\text{phi})^{3+}$ and $\text{Ru}(\text{bpy})_2(\text{eilat})^{2+}$ are evident on the mismatched duplex. In the absence of Ru, Rh photocleavage on the mismatched duplex is most intense at the mismatched site, C16. However, with increasing Ru, it is photocleavage at this mismatched site that is preferentially inhibited; cleavage at the mismatched site is competed out at noticeably lower concentrations of $\text{Ru}(\text{bpy})_2(\text{eilat})^{2+}$ (~5 μM) than at the other matched sites. This differential inhibition is most evident in the line plot and gel quantitation graph of the titration (**Figures 4.9 and 4.10**). The higher photocleavage for $\text{Rh}(\text{bpy})_2(\text{phi})^{3+}$ in the absence of Ru actually reflects a slightly higher affinity for the mismatched site versus matched sites, a common characteristic of classical intercalators.⁴⁹

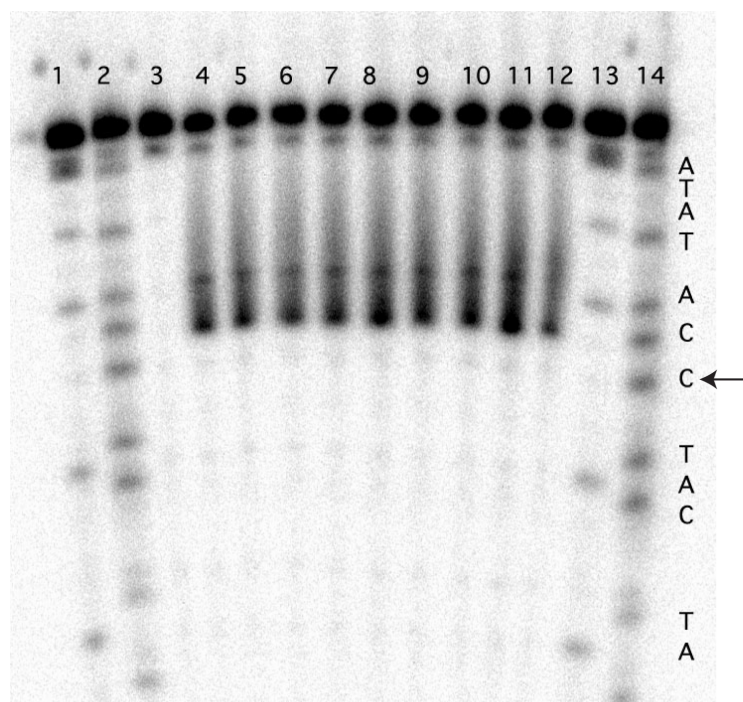


Figure 4.11: Rh(bpy)₂(chrysi)³⁺ vs. Ru(bpy)₃²⁺ competition experiment. Denaturing polyacrylamide gel showing the competition of Rh(bpy)₂(chrysi)³⁺ and Ru(bpy)₂(eilatin)²⁺ for mismatched DNA of the sequence 3'-GCGATGCAGATATACCTACTAGGATTCAGTGCATG-³²P-5' (the italicized C is complementary to another C). All samples were prepared with 0.66 μM DNA, 50 mM NaCl, 10 mM NaPi, pH 7.1 and, unless otherwise stated, irradiated for 6 minutes on a solar simulator. Lanes 1, 2, 13, and 14 are Maxam-Gilbert sequencing reactions for A+G and C+T, respectively. Lane 3 is a light control showing DNA irradiated in the absence of metal complex. Lanes 4–12 contain 0.66 μM Rh(bpy)₂(chrysi)³⁺ and increasing concentrations of Ru(bpy)₃²⁺: 0, 0.1, 0.33, 0.66, 1, 2, 3.3, 5, 15, and 33 μM respectively. Wide photocleavage bands do not reflect non-specific photocleavage at more than one site but rather the multiple products produced by hydrogen abstraction upon photo-activated cleavage at the mismatched site. The arrow marks the mismatched site.

Preferential inhibition of Rh photocleavage by $\text{Ru}(\text{bpy})_2(\text{eilatin})^{2+}$ may similarly reflect this preferential stacking with a mismatched site. Indeed, the gel quantitation shows that binding to the mismatch is less than an order of magnitude tighter than to matched sites. Curiously, the T13 cleavage site is also competed out by the Ru complex well before the other matched locations. Since hyper-reactivity of $\text{Rh}(\text{bpy})_2(\text{phi})^{3+}$ at T13 likely depends on the nearby C16 mismatch, it appears it is similarly affected by competition with $\text{Ru}(\text{bpy})_2(\text{eilatin})^{2+}$.

4.2.3: DETERMINING THE MISMATCH-SPECIFIC BINDING AFFINITY OF $\text{RU}(\text{BPY})_2(\text{EILATIN})^{2+}$

While competition experiments with a non-specific intercalator provides qualitative information about site preference, quantitative data regarding site-specific affinity can be determined by competition with a mismatch-specific metalloinsertor, $\text{Rh}(\text{bpy})_2(\text{chrysi})^{3+}$. For this second competition experiment, a similar but shorter 5'- ^{32}P -labeled oligonucleotide was synthesized to minimize non-specific binding to matched DNA. Complements containing a guanine and cytosine across from a central cytosine (bold) were also synthesized to afford matched (ES-M) and mismatched (ES-MM) duplexes: 5'- ^{32}P -TTAGGATCATCCATATA-3'. A titration employing 1 μM mismatched DNA in buffer (50 mM NaCl, 10 mM NaPi, pH 7.1) and variable $\text{Rh}(\text{bpy})_2(\text{chrysi})^{3+}$ was first used to obtain a mismatch-specific binding constant for the rhodium complex of $1.7(2) \times 10^6 \text{ M}^{-1}$ (**Figure 4.12**).

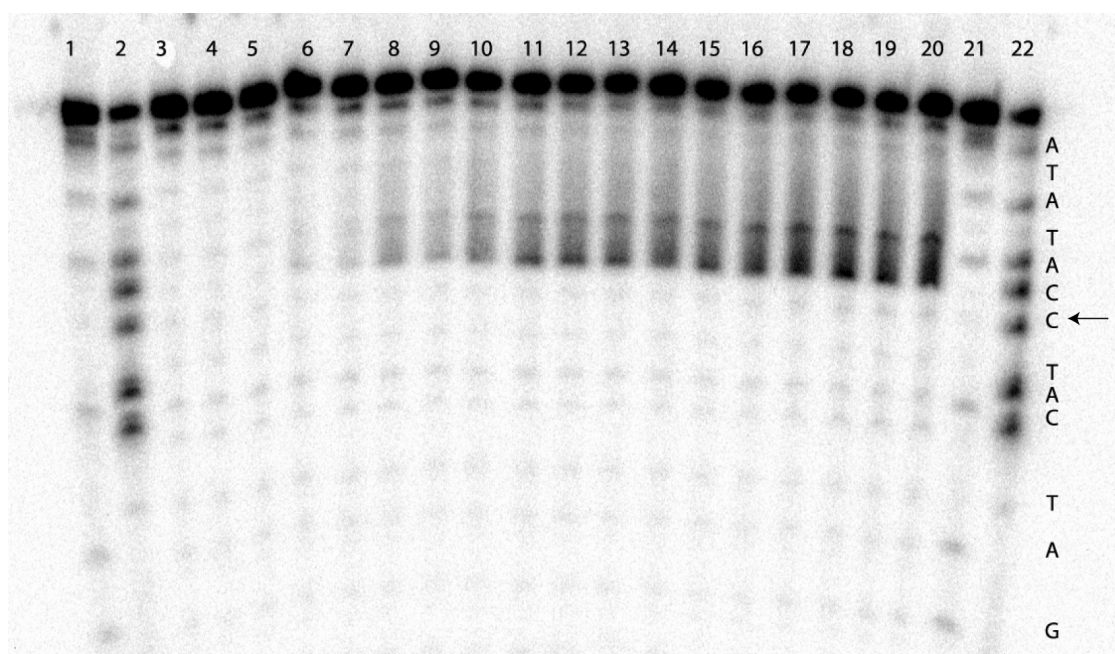


Figure 4.12: $\text{Rh}(\text{bpy})_2(\text{chrysi})^{3+}$ binding constant gel. Denaturing polyacrylamide gel showing the photocleavage titration of $\text{Rh}(\text{bpy})_2(\text{chrysi})^{3+}$ and the oligonucleotide 5'- ^{32}P -TTAGGATCATCCATATA-3' (the italicized C marks the site of the C•C mismatch). All samples were prepared with 1 μM DNA, 50 mM NaCl, 10 mM NaPi, pH 7.1 and, unless otherwise stated, irradiated for 5 minutes on a solar simulator. Lanes 1, 2, 21, and 22 are Maxam-Gilbert sequencing reactions for A+G and C+T, respectively. Lane 3 is a light control displaying DNA irradiated in the absence of metal complex. Lane 4 is a dark control displaying DNA incubated with metal complex without irradiation. Lanes 5–20 contain increasing concentrations of $\text{Rh}(\text{bpy})_2(\text{chrysi})^{3+}$: 0, 0.1, 0.2, 0.3, 0.4, 0.5, 0.6, 0.7, 0.8, 0.9, 1, 2, 3, 4, 5 μM , respectively. Wide photocleavage bands do not reflect non-specific photocleavage at more than one site but rather the multiple products produced by hydrogen abstraction upon photo-activated cleavage at the mismatched site. The arrow marks the mismatched site.

Given a known specific binding constant for $\text{Rh}(\text{bpy})_2(\text{chrysi})^{3+}$, a competition experiment with $\text{Ru}(\text{bpy})_2(\text{eilatin})^{2+}$ can yield the quantitative binding affinity of the Ru complex for the mismatched site.^{50, 51} The competition experiment was performed using 3 μM ES-MM DNA and 3 μM $\text{Rh}(\text{bpy})_2(\text{chrysi})^{3+}$ in 50 mM NaCl, 10 mM NaPi, pH 7.1 along with increasing concentrations of $\text{Ru}(\text{bpy})_2(\text{eilatin})^{2+}$ (0–20 μM). The samples were then irradiated for 15 minutes on a solar simulator and subsequently eluted through a denaturing polyacrylamide gel. The resultant gel clearly shows initially strong $\text{Rh}(\text{bpy})_2(\text{chrysi})^{3+}$ photocleavage at the mismatch site that is inhibited by increasing concentrations of $\text{Ru}(\text{bpy})_2(\text{eilatin})^{2+}$ (**Figures 4.13** and **4.14**). From these titration data we can extract a C•C mismatch-specific binding constant for $\text{Ru}(\text{bpy})_2(\text{eilatin})^{2+}$ of $2.2(2) \times 10^6 \text{ M}^{-1}$.^{50, 51} It is interesting that the Ru affinity for this mismatched site is comparable to that of $\text{Rh}(\text{bpy})_2(\text{chrysi})^{3+}$. Note that this value reflects binding to a 15-mer that contains additional matched sites to which the Ru complex may also bind (albeit likely at higher Ru concentrations). As a result, the binding affinity for the mismatched site must be considered in the context of competition also with matched sites.

4.2.4: IMPLICATIONS FOR METALLOINSERTOR DESIGN

Taken together, the two competition experiments clearly indicate that while $\text{Ru}(\text{bpy})_2(\text{eilatin})^{2+}$ does show some preference for binding the C•C mismatch, the bulky complex also displays significant binding to well-matched B-form DNA sites. The site-specificity of the Ru complex for a mismatch is therefore significantly less than that of $\text{Rh}(\text{bpy})_2(\text{chrysi})^{3+}$. A comparison of the measured mismatched-site dissociation constant ($K_D = 460(9) \text{ nM}$) to those reported for matched sites supports this assertion;

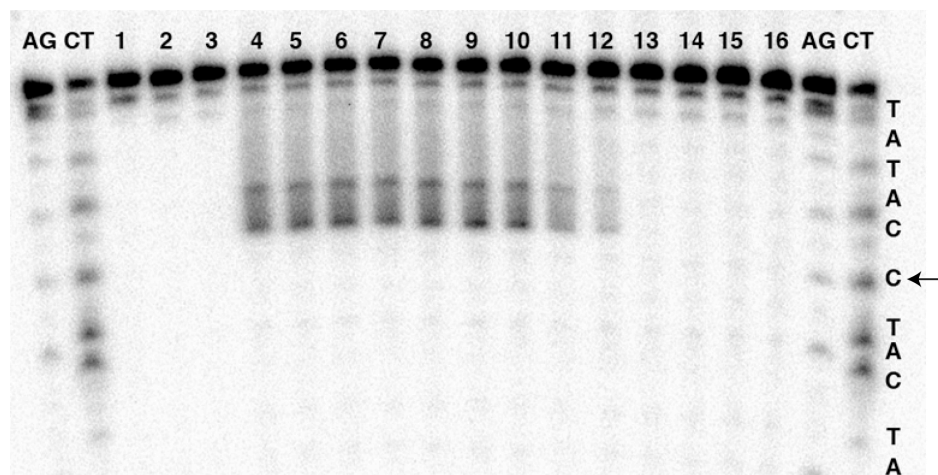


Figure 4.13: Rh(bpy)₂(chrysi)³⁺ vs. Ru(bpy)₂(eilatin)²⁺ competition experiment.

Denaturing polyacrylamide gel of a competition experiment between Rh(bpy)₂(chrysi)³⁺ and Ru(bpy)₂(eilatin)²⁺ for a CC mismatch in the oligonucleotide 5'-³²P-TTAGGATCATCCATATA-3'.

AG and CT lanes are Maxam Gilbert sequencing reactions. All samples contained 3 μM mismatched duplex in a buffer of 50 mM NaCl, 10 mM NaPi, pH 7.1 and were irradiated for 10 minutes using a solar simulator unless otherwise stated. Sample conditions: lane 1, DNA only irradiated without Rh; lane 2, 3 μM Rh(bpy)₂(chrysi)³⁺ without irradiation; lane 3, 3 μM Ru(bpy)₂(eilatin)²⁺ irradiated without Rh; lanes 4–16, 3 μM Rh(bpy)₂(chrysi)³⁺ and increasing concentrations of Ru(bpy)₂(eilatin)²⁺, 0, 0.1, 0.33, 0.66, 1, 2, 3, 5, 10, 20, 33, 66, 100 μM, respectively. Wide photocleavage bands do not reflect non-specific photocleavage at more than one site but rather the multiple products produced by hydrogen abstraction upon photo-activated cleavage at the mismatched site. The arrow marks the mismatched site.

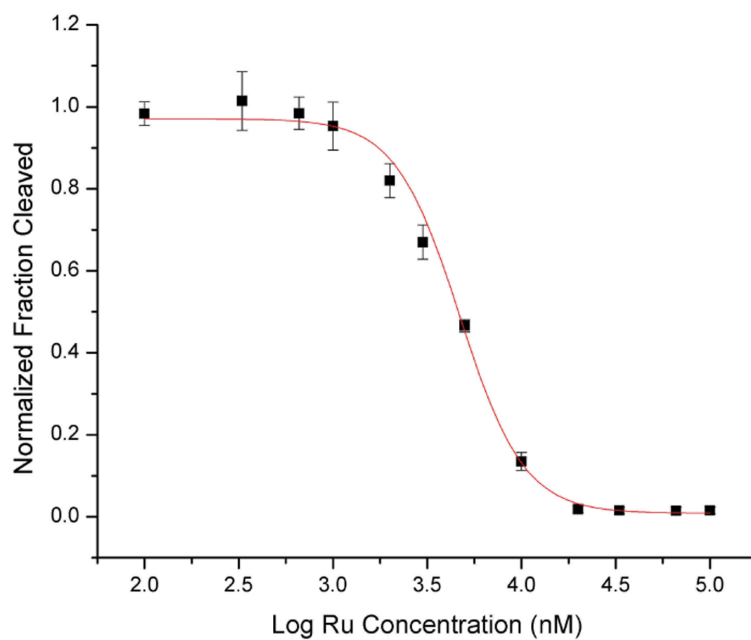
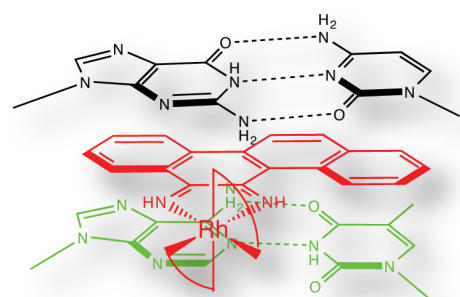


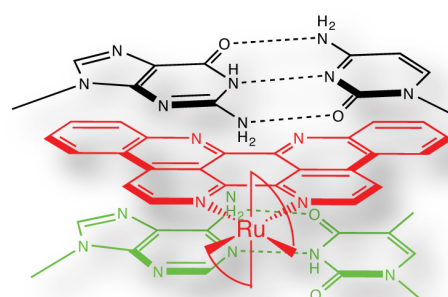
Figure 4.14: $\text{Rh}(\text{bpy})_2(\text{chrysi})^{3+}$ vs. $\text{Ru}(\text{bpy})_2(\text{eilatin})^{2+}$ competition experiment. Competitive binding of $\text{Ru}(\text{bpy})_2(\text{eilatin})^{2+}$ to mismatched DNA monitored using $\text{Rh}(\text{bpy})_2(\text{chrysi})^{3+}$ photocleavage. The plot shows fraction DNA cleaved against $\text{Ru}(\text{bpy})_2(\text{eilatin})^{2+}$ concentration for four trials of the competition experiment.

with matched DNA, binding is in the low micromolar range.³⁶⁻³⁸ Thus the selectivity of the complex for mismatched sites is modest (ratio of binding mismatched versus matched ≤ 10). It is noteworthy that earlier it was suggested that $\text{Ru}(\text{bpy})_2(\text{eilatin})^{2+}$ may bind preferentially to large structural motifs in folded RNAs. Indeed, binding of the hydrophobic and cationic Ru complex may arise with a range of nucleic acid structures.

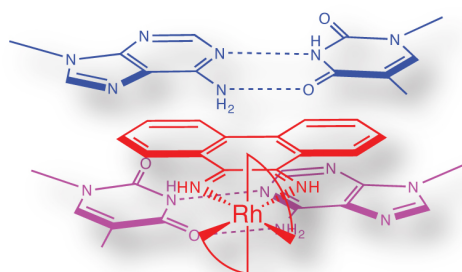
The ability of $\text{Ru}(\text{bpy})_2(\text{eilatin})^{2+}$ to bind both matched and mismatched DNA prompts the consideration of how the Ru complex may interact structurally with matched and mismatched sites. **Figure 4.15** shows schematic illustrations of $\text{Ru}(\text{bpy})_2(\text{eilatin})^{2+}$ bound to mismatched DNA in comparison to $\text{Rh}(\text{bpy})_2(\text{chrysi})^{3+}$ and to matched DNA in comparison to $\text{Rh}(\text{bpy})_2(\text{phi})^{3+}$. Binding of the Rh complexes to their target sites are based upon crystal structures and show access from the minor groove side for metalloinsertion into a mismatched site and from the major groove side for access by metallointercalation.^{11, 16} For the Rh complexes, it is apparent that these binding modes permit complete stacking of the inserting ligand between the base pairs. Moreover, the ancillary ligands of the octahedral complexes provide a barrier both to deeper insertion and significant rotation in the pocket. The complexes are bound so that the dyad axis of the base pairs bisects the immine-Rh-immine angle. In this mode, binding of the complexes is optimized for stacking, both at the mismatched and matched site. As illustrated in **Figure 4.15**, the Ru complex is also well situated within a mismatched site for substantial stacking overlap. Overlap with the base pairs is quite comparable for the chrysi and eilatin ligands, consistent with their similar binding affinity for the C•C mismatch. Significantly for $\text{Ru}(\text{bpy})_2(\text{eilatin})^{2+}$, however, the complex can still stack well within a matched site, although rotated relative to the bound Rh complex.



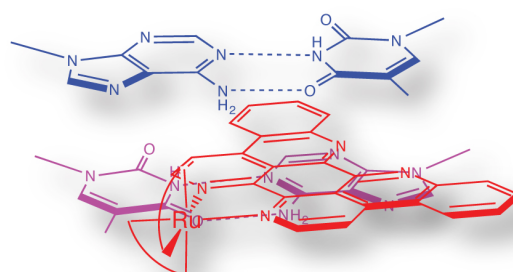
Chrysi Mismatched Site Binding: Insertion from Minor Groove
(bases extruded by inserting ligand not shown)



Eilatin Mismatched Site Binding: Insertion from Minor Groove
(bases extruded by inserting ligand not shown)



Phi Matched Site Binding: Intercalation from Major Groove



Eilatin Matched Site Binding: Intercalation from Major Groove

Figure 4.15: Proposed binding model for $\text{Ru}(\text{bpy})_2(\text{eilatin})^{2+}$ with matched and mismatched DNA. Schematic illustrations of $\text{Ru}(\text{bpy})_2(\text{eilatin})^{2+}$ (right) bound to mismatched (top) and matched (bottom) DNA sites based on the crystal structures of a chrysi (top left) and phi complex (bottom left) of Rh bound to mismatched and matched DNA, respectively. For binding to the mismatched site, the metal complexes are oriented from the minor groove side, whereas for binding to the matched site, the association is from the major groove side.

The eilatin ligand is sufficiently expansive that substantial stacking is available between the base pairs without a straight-on orientation of the complex. It is noteworthy that we have seen previously for $\text{Ru}(\text{bpy})_2\text{dppz}^{2+}$ (dppz = dipyridophenazine) fluorescence and NMR results that are consistent with a mixture of straight-on and side-on orientations in matched duplex DNA.⁵² Here, at the matched site, the eilatin complex can easily rotate within the intercalation site and maintain significant overlap with the bases above and below. Indeed, the stacking area appears comparable to that of the phi complex, just as their binding affinities for matched sites are similar. The great expanse of the eilatin ligand permits this significant stacking without the axial ligands serving as a barrier to rotation. Thus, while binding to a mismatched site by $\text{Ru}(\text{bpy})_2(\text{eilatin})^{2+}$ is preferred, binding to matched sites is not precluded.

4.3: CONCLUSIONS

These studies show that simply increasing the expanse of a metalloinsertor is not sufficient to gain an increase in specific binding to a mismatched site in duplex DNA. While binding to a mismatched site is still preferred by a complex with a bulkier ligand, the increased expanse also provides stacking area for the complex at a matched site if the ligand is particularly large. In comparing the family of bulky metal complexes, similar affinities in binding mismatched DNA are observed for those bearing the phzi and chrysi ligands versus that containing the even more expansive eilatin ligand. With $\text{Ru}(\text{bpy})_2(\text{eilatin})^{2+}$, however, we see that specificity for a single base pair mismatch is lost. That the eilatin ligand extends considerably from the metal center in two directions is likely responsible for this loss in specificity for mismatched sites and gain in affinity

for matched DNA. Clearly, the structural characteristics of $\text{Ru}(\text{bpy})_2(\text{eilatin})^{2+}$ allow the complex to bind matched DNA in a manner that $\text{Rh}(\text{bpy})_2(\text{chrysi})^{3+}$ and $\text{Rh}(\text{bpy})_2(\text{phzi})^{3+}$ cannot. As a consequence, then, these experiments teach us something simple about the design of mismatch-recognition ligands: bulky is good, but bulkier is not necessarily better.

4.4: EXPERIMENTAL PROTOCOLS

Many of the procedural details for this investigation are included in Chapter 2 of this text. These include the following: the synthesis of $\text{Rh}(\text{bpy})_2(\text{chrysi})^{3+}$ (2.3.2.5); the synthesis of $\text{Rh}(\text{bpy})_2(\text{phi})^{3+}$ (2.3.2.7); the synthesis, purification, and radiolabeling of oligonucleotides (2.4.1–2.4.2); the Maxam-Gilbert sequencing of radiolabeled DNA (2.4.3); the execution of binding constant titrations (2.4.4.2); the performance of competition experiments with non-specific metallointercalators (2.4.4.3); and the performance of competition experiments with site-specific metalloinsertors (2.4.4.3). Further experimental details of the competition experiments can be found in their corresponding figure captions.

4.4.1: MATERIALS AND INSTRUMENTATION

All reagents were obtained from commercial sources and used as received without further purification. RhCl_3 and RuCl_3 were purchased from Pressure Chemicals. $\text{Rh}(\text{bpy})_2(\text{phi})^{3+}$ and $\text{Rh}(\text{bpy})_2(\text{chrysi})^{3+}$ were synthesized according to published protocols.³² All non-aqueous solvents were purchased from Fluka and stored under argon

and over molecular sieves. All water used was purified using a MilliQ water purification system. Unless otherwise noted, all reactions were performed under ambient conditions.

$^1\text{H-NMR}$ spectra were recorded on a Varian 300 MHz spectrometer at room temperature using solvent residual signal as a reference to TMS. Mass spectrometry was performed at either the Caltech mass spectrometry facility or in the Beckman Institute Protein/Peptide Micro Analytical Laboratory (PPMAL). Absorption spectra were recorded on a Beckman DU 7400 spectrophotometer. Extinction coefficients for $\text{Ru}(\text{bpy})_2(\text{eilatin})^{2+}$ were determined using inductively coupled plasma mass spectrometry.

Oligonucleotides were synthesized on an ABI 3400 DNA synthesizer and purified via HPLC in duplicate (DMT-OFF and DMT-ON) before use. All reverse-phase HPLC purifications were performed on an HP1100 high-pressure liquid chromatography system equipped with a diode array detector using a Varian DynaMax C18 semipreparative column (see Chapter 2, section 2.4.1). Irradiations were performed using an Oriel Instruments solar simulator (320–440 nm). All PAGE experiments described employed denaturing 20% polyacrylamide gels (SequaGel, National Diagnostics) and were performed according to published procedures. Gels were developed using Molecular Dynamics phosphorimaging screens and a Molecular Dynamics Storm 820 phosphorimager and were subsequently visualized and quantified with Molecular Dynamics ImageQuant software.

4.4.2: SYNTHESIS OF EILATIN

Eilatin was synthesized according to the biomimetic synthesis published by Gellerman, et al. (see **Figure 4.4**).⁴¹⁻⁴³

4.4.2.1: SYNTHESIS OF KYNURAMINE TRIFLUOROACETAMIDE

In a 25 mL round-bottom flask, kynuramine (250 mg, 1.5 mmol) and ethyl trifluoroacetate (710 mg, 5 mmol) were dissolved in 6 mL MeOH. The resultant solution was stirred at room temperature for 4 h. After 4 h, the solution was dried via rotary evaporation. The residue was then taken up in 98:2 CH₂Cl₂:H₂O, washed 3 times with 50 mL NaHCO_{3(aq)}, dried with MgSO₄, and filtered. The organic phase was then dried *in vacuo* to yield the product as a yellow oil (300 mg, 77%).

ESI-MS: 260 [M+H]⁺, 282 [M+Na]⁺

4.4.2.2: SYNTHESIS OF 1,2-ACRIDINEDIONE INTERMEDIATE

In a 100 mL round-bottom flask, kynuramine trifluoroacetamide (200 mg, 0.76 mmol), catechol (37 mg, 0.34 mmol, 0.5 equiv.), and NaIO₃ (1.5 g, 7.7 mmol, 10 equiv.) were dissolved in 50 mL 9.5:1 EtOH:H₂O. The reaction mixture was cloudy at first and was stirred for 48 h. Over the course of the reaction, the mixture turned dark brown. After 48 h, the solvent was removed via rotary evaporation. The residue was taken up in CH₂Cl₂ and purified via column chromatography (SiO₂, 4:1 EtOAc:Hex). After purification, the product was isolated as an orange oil (350 mg, 0.57 mmol, 76%).

ESI-MS: 606 [M+H]⁺, 628 [M+Na]⁺

4.4.2.3: SYNTHESIS OF EILATIN

In a 25 mL round-bottom flask, the 1,2-acridinedione intermediate (50 mg, 0.08 mmol) was dissolved in 10 mL MeOH and 2 mL NH₄OH. The reaction mixture was stirred at room temperature for 24 hours. After 24 hours, the solution was concentrated *in vacuo*, and the residue was taken up in a minimum volume of MeOH. The reaction mixture was then purified via preparative TLC (SiO₂, 96:4 CHCl₃:MeOH) to yield the desired product as a yellow oil (20 mg, 0.05 mmol, 63%).

ESI-MS: 356 [M+H]⁺, 369 [M+Na]⁺

¹H-NMR (d₆-DMSO): 9.32 ppm (d, 2H); 8.70 ppm (d, 2H); 8.68 ppm (d, 2H); 8.57 ppm (d, 2H); 8.00 ppm (d, 2H); 7.87 ppm (d, 2H);

UV-Vis (MeOH, **Figure 4.16**): λ_{max} 242 nm (ε = 48,200), 286 (ε = 36,700), 366 (ε = 11,500), 388 (ε = 21,000), 408 (ε = 30,400), and 434 (ε = 27,000).

4.4.3: SYNTHESIS OF RU(BPY)₂(EILATIN)²⁺

4.4.3.1: SYNTHESIS OF RU(BPY)₂Cl₂

In a 50 mL round-bottom flask, RuCl₃ (0.52 g, 2.5 mmol), 2,2'-bipyridine (0.8 g, 5.0 mmol), LiCl (0.85 g, excess) were suspended in 10 mL and DMF. Reflux the reaction mixture for 8 h at 180 °C. After 8 h, the suspension was allowed to cool to room temperature and poured into 80 mL of stirring acetone. The reaction vessel was washed 2 times with 10 mL acetone. The combined acetone fractions were cooled to 4 °C overnight to prompt crystallization. After 16 h, the solution was vacuum filtered to isolate the dark purple precipitate, which was subsequently washed with water (3 x 10 mL) and diethyl ether (3 x 10 mL).

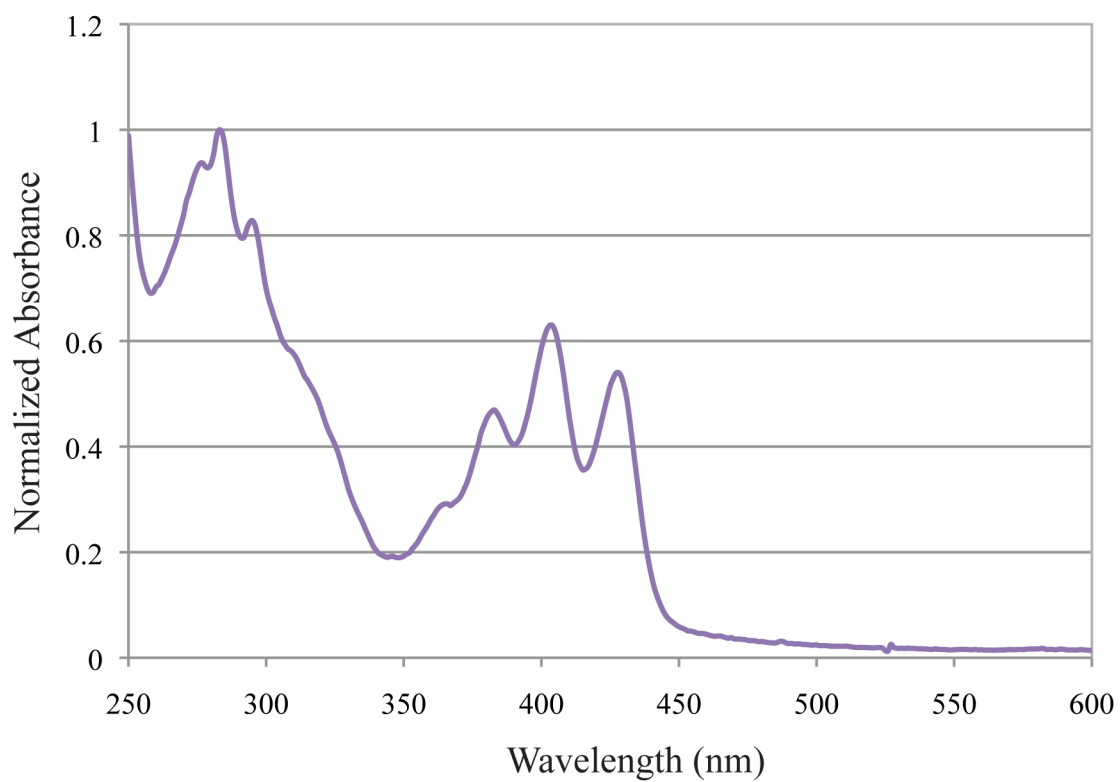


Figure 4.16: UV-Vis spectrum of eilatin. Extinction coefficients: λ_{\max} 286 ($\epsilon = 36,700$), 366 ($\epsilon = 11,500$), 388 ($\epsilon = 21,000$), 408 ($\epsilon = 30,400$), and 434 ($\epsilon = 27,000$)

ESI-MS: 478 [M+H]⁺, 450 [M-Cl]⁺

¹H-NMR (d₆-DMSO): 9.95 ppm (d, 2H); 8.60 ppm (d, 2H); 8.48 ppm (d, 2H); 8.05 ppm (t, 2H); 7.75 ppm (t, 2H); 7.65 ppm (t, 2H); 7.50 ppm (d, 2H); 7.08 ppm (t, 2H).

4.4.3.2: SYNTHESIS OF Ru(BPY)₂(EILATIN)²⁺

In a 100 mL round-bottom flask, Ru(bpy)₂(Cl)₂ (10 mg, 0.02 mmol) and eilatin (10 mg, 0.03 mmol) were dissolved in 20 mL MeOH and 5 mL H₂O. The resultant solution was refluxed at 100 °C for 4 h. After 4 h, the solvent was removed via rotary evaporation, the residue was re-dissolved in H₂O to form a greenish solution, and the product was precipitated via addition of excess NH₄PF₆. The suspension was vacuum filtered, and the dark green precipitate was washed with copious water.

The product precipitate was taken up in acetonitrile and anion exchanged on a Sephadex QAE-25 column that had been pre-equilibrated with 0.05 M MgCl₂. The resultant green solution was concentrated on a reverse phase C-18 cartridge, washed, eluted, and lyophilized to dryness. Finally, the green solid was taken up in H₂O and purified via reverse-phase high-performance liquid chromatography using an HP1100 HPLC system, a Varian DynaMax C18 semipreparative column, and an elution gradient of 85:15 to 40:60 H₂O (0.1% TFA):MeCN (0.1% TFA) over 60 min.

ESI-MS (m/z): 768 [M-2H]⁺, 385 [M-H]²⁺

¹H-NMR (d₆-DMSO): 8.93 ppm (d, 2H); 8.77 ppm (d, 2H); 8.74 (d, 2H); 8.29 (m, 2H); 8.17 ppm (d, 2H); 8.14 ppm (d, 2H); 8.08 (m, 2H); 7.96 (m, 2H); 7.88 (d, 2H); 7.69 (m, 2H).

UV-Vis (H₂O, pH 7.0): λ_{max} 244 nm ($\epsilon = 64,000$), 287 nm ($\epsilon = 68,000$), 426 nm ($\epsilon = 38,000$).

4.5: REFERENCES

1. Erkkila, K. E.; Odom, D. T.; Barton, J. K. *Chemical Reviews* **1999**, *99* (9), 2777–2795.
2. Zeglis, B. M.; Pierre, V. C.; Barton, J. K. *Chemical Communications* **2007**, 4565–4579.
3. Ruba, E.; Hart, J. R.; Barton, J. K. *Inorganic Chemistry* **2004**, *43* (15), 4570–4578.
4. Junicke, H.; Hart, J. R.; Kisko, J. L.; Glebov, O.; Kirsch, I. R.; Barton, J. K. *Proceedings of the National Academy of Sciences U. S. A.* **2003**, *100*, 3737–3742.
5. Schatzschneider, U.; Barton, J. K. *Journal of the American Chemical Society* **2004**, *126* (28), 8630–8631.
6. Petitjean, A.; Barton, J. K. *Journal of the American Chemical Society* **2004**, *126* (45), 14728–14729.
7. Brunner, J.; Barton, J. K. *Biochemistry* **2006**, *45* (40), 12295–12302.
8. Zeglis, B. M.; Barton, J. K. *Journal of the American Chemical Society* **2006**, *128* (17), 5654–5655.
9. Ernst, R. J.; Song, H.; Barton, J. K. *Journal of the American Chemical Society* **2009**, *131* (6), 2359–2366.
10. Cordier, C.; Pierre, V. C.; Barton, J. K. *Journal of the American Chemical Society* **2007**, *129*, 12287–12295.

11. Pierre, V. C.; Kaiser, J. T.; Barton, J. K. *Proceedings of the National Academy of Sciences U. S. A.* **2007**, *103*, 429–434.
12. Collins, J. G.; Shields, T. P.; Barton, J. K. *Journal of the American Chemical Society* **1994**, *116* (22), 9840–9846.
13. Franklin, S. J.; Barton, J. K. *Biochemistry* **1998**, *37* (46), 16093–16105.
14. Hudson, B. P.; Barton, J. K. *Journal of the American Chemical Society* **1998**, *120* (28), 6877–6888.
15. Hudson, B. P.; Dupureur, C. M.; Barton, J. K. *Journal of the American Chemical Society* **1995**, *117* (36), 9379–9380.
16. Kielkopf, C. L.; Erkkila, K. E.; Hudson, B. P.; Barton, J. K.; Rees, D. C. *Nature Structural Biology* **2000**, *7* (2), 117–121.
17. Krotz, A. H.; Kuo, L. Y.; Barton, J. K. *Inorganic Chemistry* **1993**, *32* (26), 5963–5974.
18. Jackson, B. A.; Alekseyev, V. Y.; Barton, J. K. *Biochemistry* **1999**, *38* (15), 4655–4662.
19. Jackson, B. A.; Barton, J. K. *Journal of the American Chemical Society* **1997**, *119* (52), 12986–12987.
20. Jackson, B. A.; Barton, J. K. *Biochemistry* **2000**, *39* (20), 6176–6182.
21. Jackson, B. A.; Henling, L. M.; Barton, J. K. *Inorganic Chemistry* **1999**, *38* (26), 6218–6224.
22. Rudi, A.; Kashman, Y.; Gut, D.; Lellouche, F.; Kol, M. *Chemical Communications* **1997**, (1), 17–18.

23. Rudi, A.; Benayahu, Y.; Goldberg, I.; Kashman, Y. *Tetrahedron Letters* **1988**, *29* (50), 6655–6656.
24. Nakahara, S.; Tanaka, Y.; Kubo, A. *Heterocycles* **1993**, *36* (5), 1139–1144.
25. Blanco, M. D.; Avendano, C.; Menendez, J. C. *Tetrahedron* **1999**, *55* (43), 12637–12646.
26. Einat, M.; Lishner, M.; Amiel, A.; Nagler, A.; Rudi, A.; Kashman, Y.; Fabian, I. *Experimental Hematology* **1994**, *22* (8), 797–797.
27. Einat, M.; Lishner, M.; Amiel, A.; Nagler, A.; Yarkorli, S.; Rudi, A.; Kashman, Y.; Markel, D.; Fabian, I. *Experimental Hematology* **1995**, *23* (14), 1439–1444.
28. Ding, Q. Z.; Chichak, K.; Lown, J. W. *Current Medicinal Chemistry* **1999**, *6* (1), 1–27.
29. Lishner, M.; Shur, I.; Bleiberg, I.; Rudi, A.; Kashman, Y.; Fabian, I. *Leukemia* **1995**, *9* (9), 1543–1548.
30. McDonald, L. A.; Eldredge, G. S.; Barrows, L. R.; Ireland, C. M. *Journal of Medicinal Chemistry* **1994**, *37* (22), 3819–3827.
31. Bergman, S. D.; Gut, D.; Kol, M.; Sabatini, C.; Barbieri, A.; Barigelletti, F. *Inorganic Chemistry* **2005**, *44* (22), 7943–7950.
32. Zeglis, B. M.; Barton, J. K. *Nature Protocols* **2007**, *2* (2), 357–371.
33. Gut, D.; Goldberg, I.; Kol, M. *Inorganic Chemistry* **2003**, *42* (11), 3483–3491.
34. Gut, D.; Rudi, A.; Kopilov, J.; Goldberg, I.; Kol, M. *Journal of the American Chemical Society* **2002**, *124* (19), 5449–5456.
35. Bergman, S. D.; Frantz, R.; Gut, D.; Kol, M.; Lacour, J. *Chemical Communications* **2006**, (8), 850–852.

36. Leudtke, N. W.; Hwang, J. S.; Glazer, E. C.; Gut, D.; Kol, M.; Tor, Y. *Chembiochem* **2002**, *3* (8), 766–771.
37. Luedtke, N. W.; Hwang, J. S.; Nava, E.; Gut, D.; Kol, M.; Tor, Y. *Nucleic Acids Research* **2003**, *31* (19), 5732–5740.
38. Chouai, A.; Wicke, S. E.; Turro, C.; Bacsa, J.; Dunbar, K. R.; Wang, D.; Thummel, R. P. *Inorganic Chemistry* **2005**, *44* (17), 5996–6003.
39. Friedman, A. E.; Chambron, J. C.; Sauvage, J. P.; Turro, N. J.; Barton, J. K. *Journal of the American Chemical Society* **1990**, *112* (12), 4960–4962.
40. Jenkins, Y.; Friedman, A. E.; Turro, N. J.; Barton, J. K. *Biochemistry* **1992**, *31* (44), 10809–10816.
41. Gellerman, G.; Babad, M.; Kashman, Y. *Tetrahedron Letters* **1993**, *34* (11), 1827–1830.
42. Gellerman, G.; Rudi, A.; Kashman, Y. *Tetrahedron Letters* **1993**, *34* (11), 1823–1826.
43. Gellerman, G.; Rudi, A.; Kashman, Y. *Tetrahedron* **1994**, *50* (45), 12959–12972.
44. Bergman, S. D.; Kol, M. *Inorganic Chemistry* **2005**, *44* (6), 1647–1654.
45. Bergman, S. D.; Reshef, D.; Frish, L.; Cohen, Y.; Goldberg, I.; Kol, M. *Inorganic Chemistry* **2004**, *43* (13), 3792–3794.
46. Chow, C. S.; Barton, J. K. *Methods in Enzymology* **1992**, *212*, 219–242.
47. Pyle, A. M.; Long, E. C.; Barton, J. K. *Journal of the American Chemical Society* **1989**, *111* (12), 4520–4522.
48. Lim, M. H.; Lau, I. H.; Barton, J. K. *Inorganic Chemistry* **2007**, *46*, 9528–9530.
49. Jackson, B. A. Thesis, California Institute of Technology, Pasadena, CA, **2001**.

50. Hart, J. R. Thesis, California Institute of Technology, Pasadena, CA, **2006**.
51. Garbett, N. C.; Chaires, J. B. Binding: A polemic and rough guide. In *Biophysical Tools for Biologists: Vol 1 in Vitro Techniques*, Elsevier Academic Press Inc: San Diego, **2008**, Vol. 84, 3–23.
52. Dupureur, C. M.; Barton, J. K. *Journal of the American Chemical Society* **1994**, *116* (22), 10286–10287.